Ultrasound in Med. & Biol., Vol. 30, No. 10, pp. 1269-1280, 2004

0301-5629/04/$–see front matter

ELSEVIER

doi:10.1016/j.ultrasmedbio.2004.07.003

● *Original Contribution*

AN EXPERIMENTAL CHARACTERIZATION OF ELASTOGRAPHIC SPATIAL RESOLUTION: ANALYSIS OF THE TRADE-OFFS BETWEEN SPATIAL RESOLUTION AND CONTRAST-TO-NOISE RATIO

S. SRINIVASAN,*† R. RIGHETTI *† and J. OPHIR*†

*The University of Texas Medical School, Department of Radiology, Ultrasonics Laboratory, Houston, TX, USA; and †University of Houston, Electrical and Computer Engineering Department, Houston, TX, USA

(*Received* 17 *December* 2003; *revised* 18 *June* 2004; *accepted* 8 *July* 2004)

Abstract—An experimental study of the spatial resolution in elastography was conducted. Models that involved two cylindrical inclusions arranged as a wedge were used to characterize the axial and lateral resolution of the axial strain elastograms. A study of the dependence of the spatial resolution on several factors such as the algorithmic parameters, the applied strain and the modulus contrast was performed. The axial resolution was found to show a linear dependence with respect to the algorithmic parameters, namely the window length and the window shift used for strain estimation. The lateral resolution showed a weak dependence on the algorithmic parameters. A weak dependence of the spatial resolution on factors such as the modulus contrast and the applied strain was found. The trade-offs between the spatial resolution and the elastographic contrast-to-noise ratio (CNR_e) were then analyzed. A nonlinear trade-off between the CNR_e and the axial and lateral resolution was shown for conventional strain estimation techniques, with the CNR_e improving at a more than linear rate with respect to a linear degradation in the resolution. This study provided an experimental framework for characterizing the spatial resolution in elastography and facilitating a comparison of the CNR_e with spatial resolution.

Key Words: **Spatial resolution, CNR, SNR, Axial resolution, Lateral resolution, Strain imaging, Elastography.**

INTRODUCTION

Elastography has been well established in the literature as a strain imaging technique (Ophir et al. 1991, 1999). Elastography using ultrasound (US), in addition to being an adjunct to sonography, displays the mechanical properties of tissues, such as strain and elastic modulus, that are not available with sonography (Srinivasan et al. 2004). Conventional techniques in US elastography estimate strain as the gradient of the displacement estimates obtained through cross-correlation of the pre- and postcompression radiofrequency (RF) A-lines. The quality of the resulting strain estimates is typically quantified by several factors, such as the elastographic signal-to-noise ratio (SNR_e), the elastographic contrast-to-noise ratio (CNR_e) and the spatial resolution (R). Prior work on the SNR_e, CNR_e and axial resolution included the development of theoretical upper bounds on the SNR_e and CNR_e (Varghese and Ophir 1997, 1998) and lower bounds as well as practical limits on the axial resolution (Srinivasan et al. 2003). A simulation framework for studying the SNR_e and CNR_e (Srinivasan et al. 2003) and the spatial resolution in elastography (Alam et al. 2000; Righetti et al. 2002, 2003) was established. Methods to characterize the spatial resolution of elasticity imaging have been provided by Cook et al. (2000) and Liu and Insana (2003). However, an experimental characterization of the spatial resolution in elastography has not yet been conducted. Such characterization would help corroborate the simulation and theoretical findings as well as provide a framework for the development of experimental procedures and phantoms for studying spatial resolution in elastography.

In this work, we describe experimental models for the characterization of the spatial resolution of elastography (both axial and lateral resolution of the axial strain elastograms). Prior theoretical work (Srinivasan et al. 2003) and simulation work (Righetti et al. 2002) on axial resolution has established a linear dependence of the axial resolution on the window length and the window

Address correspondence to: Professor Jonathan Ophir, The University of Texas Medical School, Department of Radiology, Ultrasonics Laboratory, 6431 Fannin St. MSB 2.100, Houston, TX 77030 USA. E-mail: Jonathan.Ophir@uth.tmc.edu

overlap with the lower bounds provided by the ultrasonic bandwidth. The lateral resolution was shown to deteriorate linearly with the beamwidth (Righetti et al. 2003). We expect the experimental axial and lateral results to confirm these prior observations. Specifically, we hypothesize a good agreement between the experimental results and prior theoretical and simulation results on the spatial resolution in elastography. We also expect the resolution experiments to demonstrate trade-offs between the image quality factors in elastography.

The methods utilized in this paper are provided below. The results and a discussion of the results are provided subsequently.

METHODS

Theory

Prior work by Srinivasan et al. (2003) and Céspedes (1993) has established theoretical expressions for the axial and lateral resolution of elastography. The expression for the estimated value of the axial resolution (R_a) and the lateral resolution (R_l) was obtained (Appendix A of Srinivasan et al. 2003) as:

$$R_a = kW\left(1 + \frac{\Delta W}{W}\right), W > \frac{hc}{3B}, \tag{1}$$

and

$$R_l = kP, P > \frac{B_l}{1.5}, \tag{2}$$

where W and ΔW are, respectively, the window length and window shift used for strain estimation, B and B_l are, respectively, the absolute bandwidth and the beamwidth of the US system, P is the transducer element pitch, c is the speed of sound in tissue, h is a constant (typically $h > 5$) and k is a constant that represents the fractional change in the strain values between the inclusion and the background. For example, when the strain changes from 10% to 90% of the difference between the value in the background and the value in the inclusion, $k = 0.8$. It is of interest to note that the smallest value of W is dictated by the inequality of eqn (1). Hence, the lower bound on the axial resolution does not depend on W or ΔW, but rather on the system bandwidth, as evident from eqn (1). Such a result can also be observed in Righetti et al. (2002). Note that, irrespective of the algorithm used, the lower bound on the axial resolution is determined by the US bandwidth. Algorithms that do not require windowed segments, such as zero-crossing-tracking (Srinivasan and Ophir 2003), are capable of attaining the lower bound of the axial resolution. The inequality in eqn (1) arises from the fact that the smallest window length for unbiased time-delay estimation (Bendat and Piersol 1986) is directly related to the lower bound on the axial resolution and is given by the expression $BW_{\min} = k$; where k is a constant greater than 1. Equation (2) suggests that the lateral resolution does not depend on the axial strain estimation parameters.

The elastographic signal-to-noise ratio (SNR_e) is defined as the ratio of the mean value in the estimated strain (s) to the SD in the estimated strain (σ) in the elastogram. The contrast-to-noise (CNR_e) for an elastic inclusion was defined by Bilgen and Insana (1997) as:

$$\mathrm{CNR} = \frac{2(s_t - s_b)^2}{\sigma_t^2 + \sigma_b^2}, \tag{3}$$

where s_t and s_b are the mean values of the estimated strain in the target and the background, respectively, and $_t$ and $_b$ are the respective SDs of the estimated strains. Expressions for the SNR_e and CNR_e can be found in Varghese and Ophir (1997, 1998). The CNR_e and SNR_e can be expressed in terms of W, W and B (equation 17 in Srinivasan et al. (2003)) as:

$$\mathrm{CNR_e} \propto \mathrm{SNR_e^2} \propto (B)^3 W^2 \Delta W. \tag{4}$$

Equations (1) and (4) suggest a three-half-power trade-off between the SNR_e and axial resolution and a cubic trade-off between the CNR_e and axial resolution. A simulation framework for corroborating the theoretical results of SNR_e, CNR_e and the axial resolution was described in Srinivasan et al. (2003).

Experiments

Experiments were performed to corroborate the theory on 1. a uniformly elastic phantom for the SNR_e study, 2. a uniformly elastic phantom with a 20-mm diameter stiff cylindrical inclusion for the CNR_e study, with the modulus contrast varying between 1.5 and 10 (the modulus values were measured using a nanoindenter (Srinivasan et al. 2004) and 3. a uniformly elastic phantom with two 10-mm diameter cylindrical inclusions arranged as a wedge (i.e., touching each other at one end of the long-axis of the cylinder and with the largest separation at the other end of the long axis) for the axial resolution study, as shown in Fig. 1. The wedge angle was approximately 30°. Two experimental configurations were used to characterize the axial resolution. In one configuration, a cylinder was imaged axially, as shown in Fig. 1a and with the corresponding sonogram-elastogram pairs as in Fig. 1d. In the other configuration, the phantom was imaged laterally, as shown in Fig. 1b and with the corresponding sonogram-elastogram pairs as in Fig. 1e. For this type of experiment, the acquisition was made in several adjacent planes that were separated by 0.5 mm each (along the x-direction), starting from a separation between lesions of 5 mm and ending where the inclusions were no longer separable in the sono-

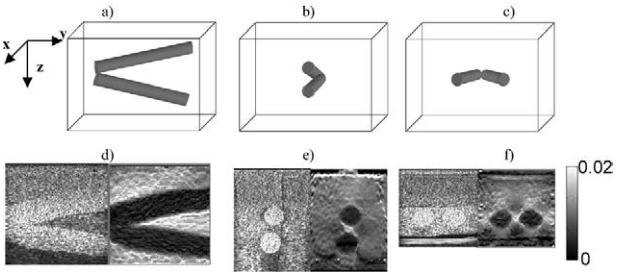

Fig. 1. (a), (b) and (c) Schematics of the two-inclusion cylindrical phantom used for the resolution study. (d) A 44 × 40 mm^2 cross-section; (e), 57 × 40 mm^2 cross-section; and (f) 37 × 40 mm^2 cross-section of the sonogram-elastogram pairs for the schematics shown in (a), (b) and (c), respectively. z, y and x = the axial, lateral and elevational directions with respect to the scanning plane. The elastograms were obtained using a window length of 2 mm and a window overlap of 80%. The color bar in (f) shows the strain range used for the display.

grams. To characterize the lateral resolution, the cylinder was imaged in the configuration shown in Fig. 1c, with the corresponding sonogram-elastogram pairs as in Fig. 1f. Here, the acquisition was made in several adjacent planes that were separated by 0.5 mm each (along the x-direction).

To evaluate the true spatial separation between lesions, the inclusions were made hyperechoic with respect to the background and the separation between them was estimated directly from the sonogram to a precision of about a wavelength in the axial direction and a pitch in the lateral direction. For the elastographic results, to estimate the separation between the inclusions, we set a strain threshold to half the strain difference between the background and the inclusion. Then we computed the number of pixels between the inclusions that exceeded this threshold. This methodology was used to determine the lower bounds on the axial resolution (Righetti et al. 2002), as well as the lateral resolution in elastography (Righetti et al. 2003). The minimum spatial separation on the elastograms that corresponded to the actual separation of the inclusions (as measured from the sonograms) was defined as the upper bound on the spatial resolution.

The background materials for the phantoms were prepared by mixing gelatin and agar in water with 6% by weight gelatin and 3% by weight agar. The inclusions were made using sponge reinforced composite material as follows. A 100 pore-per-inch (4 pore-per-mm) open-cell sponge cylinder (made of polyester material) was inserted inside the gelatin-agar-water mixture (which was prepared with 5% by weight gelatin and 2% by weight agar in deionized water at 80°C; Kallel et al. 2001). The bubbles inside the sponge were squeezed out and the sponge was allowed to retrieve back to its original size. A surfactant was added to the water to reduce its surface-tension thereby, allowing bubbles to be easily removed from the sponge. The mixture was then cooled for several hours (Kallel et al. 2001). The porosity was chosen such that the pore size allowed the gelatin to penetrate the sponge and also such that the pore size was much smaller compared with the size of the sponge sample used. These sponge reinforced phantoms offer the advantages of obtaining high modulus contrasts and sharp boundaries without specular reflections. More details on the modulus properties of the sponge reinforced phantom can be found in Srinivasan et al. (2004). The diameter of the sponge was set at 10 mm for the resolution study and 20 mm for the CNR_e study. The larger inclusion size was preferred for the CNR_e study, to obtain unbiased estimates of the variance of the strain inside the inclusion.

The acquisition was performed using an HDI-1000 (Philips Inc, Bothell, WA) US scanner, with a 128-element array, 5-MHz center frequency and a 60% fractional bandwidth transducer. The sampling frequency was set at 20 MHz. To generate the elastograms, the RF data were processed using an adaptive strain estimation algorithm (Srinivasan et al. 2002b).

We experimentally evaluated the obtainable axial and lateral elastographic resolutions, SNR_e and CNR_e, with respect to the applied strain, the signal-processing parameters (W and ΔW) and the elastic contrast. Slip boundary conditions at the compressor as well as the base were assumed. The applied strain was varied from 0.25% to 4%. The value of W was varied between 1 mm and 5 mm. The value of ΔW was varied between $0.2W$ and W. A total of 12 phantoms were used for computing the statistics with respect to the applied strain, W and ΔW. The lesion-background modulus contrast varied between 1.7 and 5 for the resolution study and between 1.7 and 10 for the CNR_e study. The modulus values inside the inclusion materials and in the background materials were measured using nanoindentation (Srinivasan et al. 2004). For each modulus contrast level, four phantoms were used and 40 realizations were acquired from the same imaging planes for each phantom. It is to be noted that the 40 realizations were obtained at the same loca-

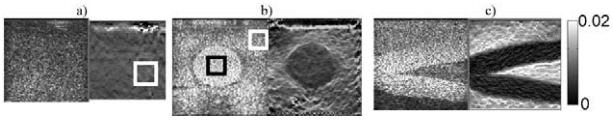

Fig. 2. Sonogram-elastogram pairs of (a) uniform phantom, (b) a phantom with a 20-mm diameter cylindrical inclusion, and (c) with two 10-mm diameter cylindrical inclusions arranged as a wedge. The elastograms were computed using $W = 2$ mm and $\Delta W = 0.2W$. The square boxes in (a) and (b) indicate the ROIs from which the SNR_e and CNR_e were computed. The color bar in (c) shows the strain range used for the display.

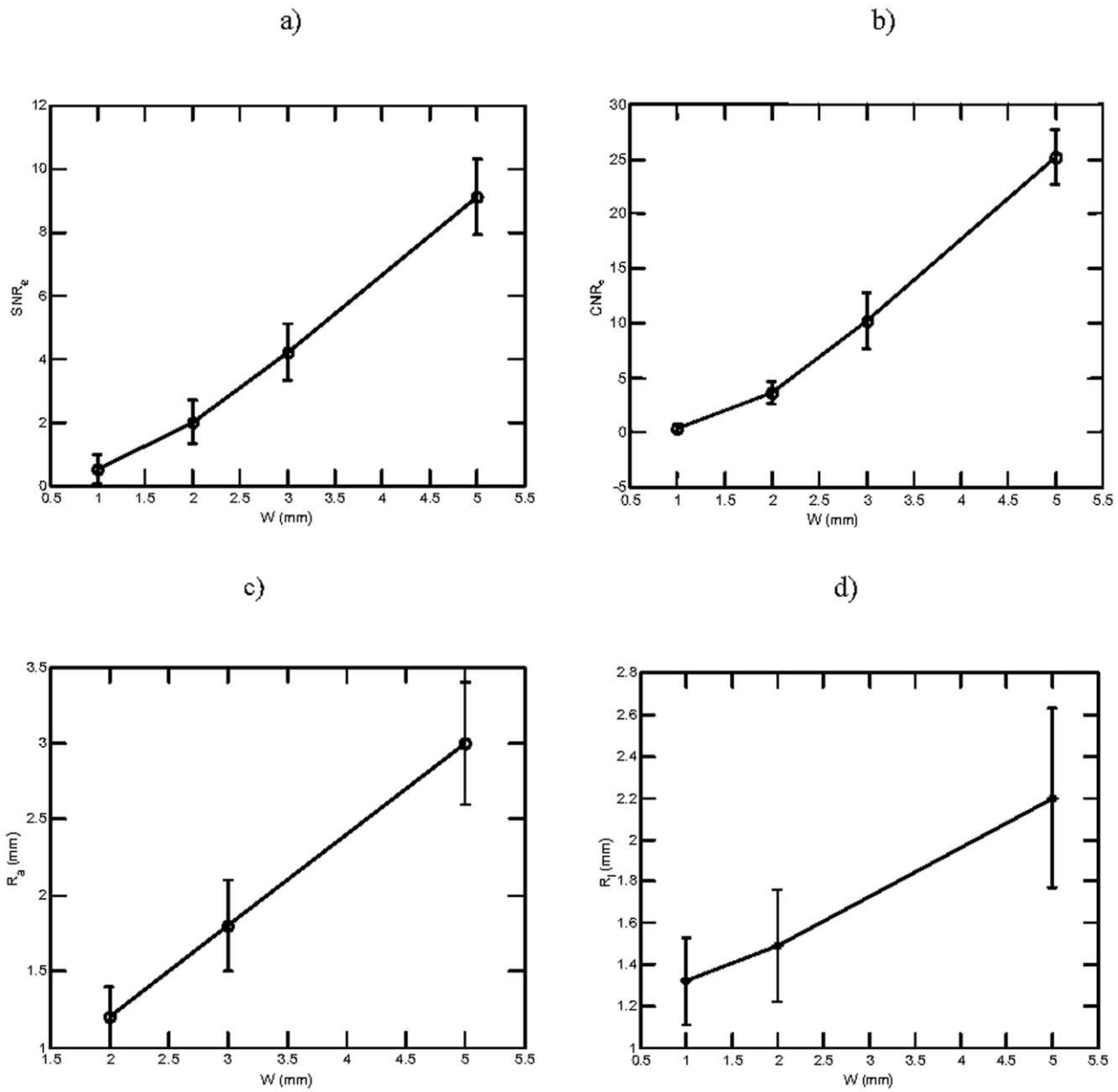

Fig. 3. (a) SNR_e, (b) CNR_e, (c) R_a and (d) R_l as a function of W (applied strain = 1%, $\Delta W = 0.2W$). The data points represent the means and the error bars are the SDs over 12 realizations.

tion of the phantom and, hence, were not independent of each other. They were used essentially to improve the sonographic SNR (Varghese and Ophir 1997) and also to reduce the noise due to digitization (Srinivasan et al. 2002a), thereby improving the accuracy of the inclusion separation in the sonograms.

Finally, the separations between the inclusions in the elastograms were compared with those corresponding to the sonograms for several parameters, such as the applied strain, W and ΔW and the elastic contrast. This was done to evaluate the accuracy of the elastographic measurements.

RESULTS

Typical sonogram-elastogram pairs for the SNR_e study, the CNR_e study and the axial resolution study are shown in Fig. 2. The elastograms for the resolution study were obtained as the average over 40 individual elastograms that were obtained at the same location in the

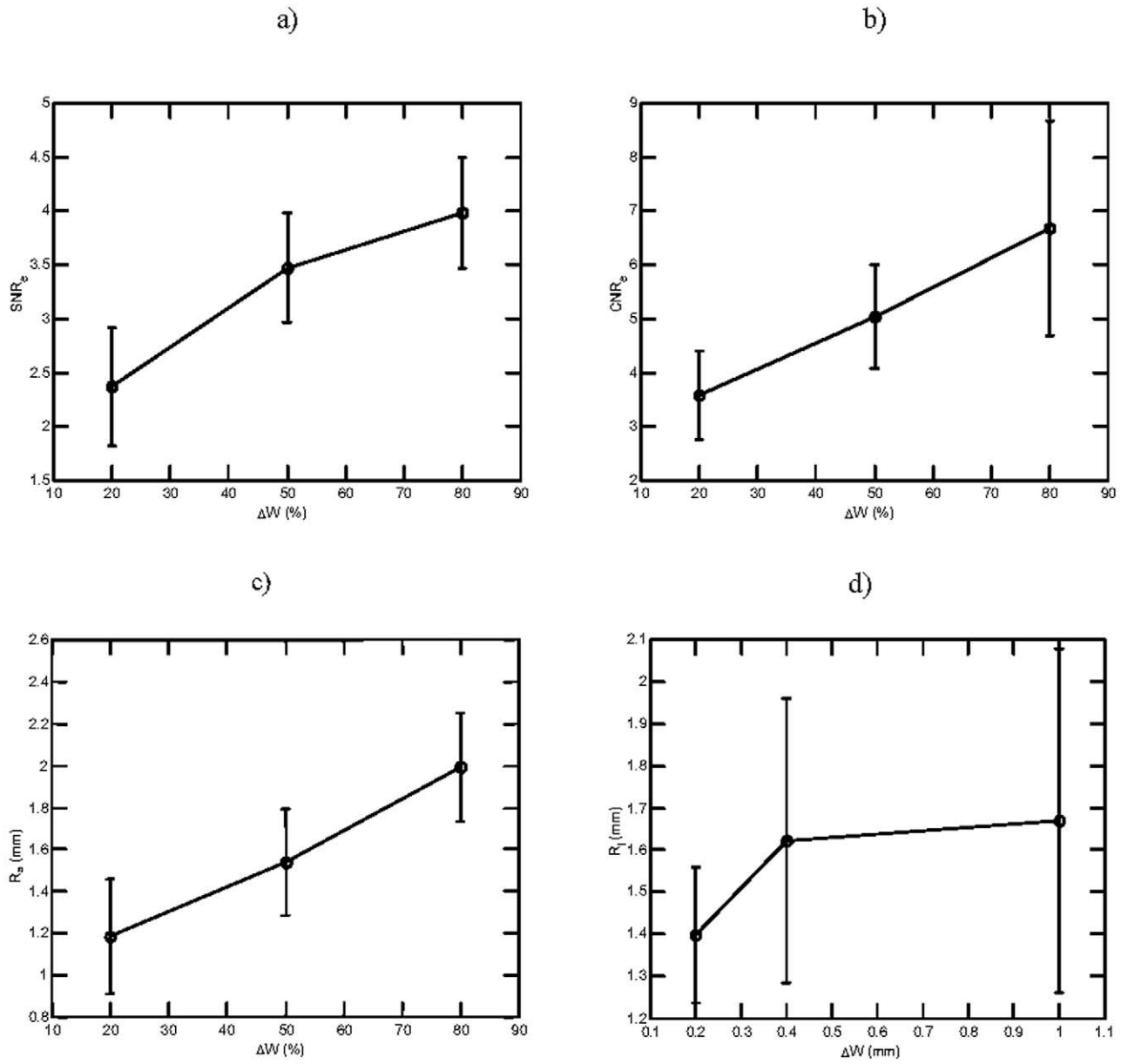

Fig. 4. (a) SNR_e, (b) CNR_e, (c) R_a and (d) R_l as a function of ΔW (applied strain = 1%, W = 2 mm). The data points represent the means and the error bars the SD over 12 realizations.

image. An applied strain of 1% was used for the subsequent experiments unless mentioned otherwise.

For the experiments, the SNR_e and CNR_e were computed from the images by choosing regions-of-interest (ROIs) and computing the strain statistics, as explained in the previous section. The axial resolution was computed by estimating the smallest separation between the two inclusions in the elastogram, as explained in the Methods section. Figure 3 shows the SNR_e, CNR_e, the axial resolution and the lateral resolution as a function of W for an applied strain of 1% and $\Delta W = 0.2W$. It can be seen that the SNR_e (Fig. 3a) and CNR_e (Fig. 3b) improve at a more than linear rate with respect to W for a value ΔW that is a fixed fraction of W. Such an increase is also predicted by eqn (4) and has been demonstrated in Srinivasan et al. (2003a). The value of R_a, on the other hand, was found to increase at a linear rate with respect to W (Fig. 3c), as predicted by eqn (1). A linear regression analysis was performed to show that the axial resolution improved linearly with W and the coefficient of determination (r) was found to be greater than 0.98. The lateral resolution showed a slight deterioration with the value of W (Fig. 3d). However, statistical significance of the changes with respect to W could not be established for the values of W considered in this study (p values > 0.05

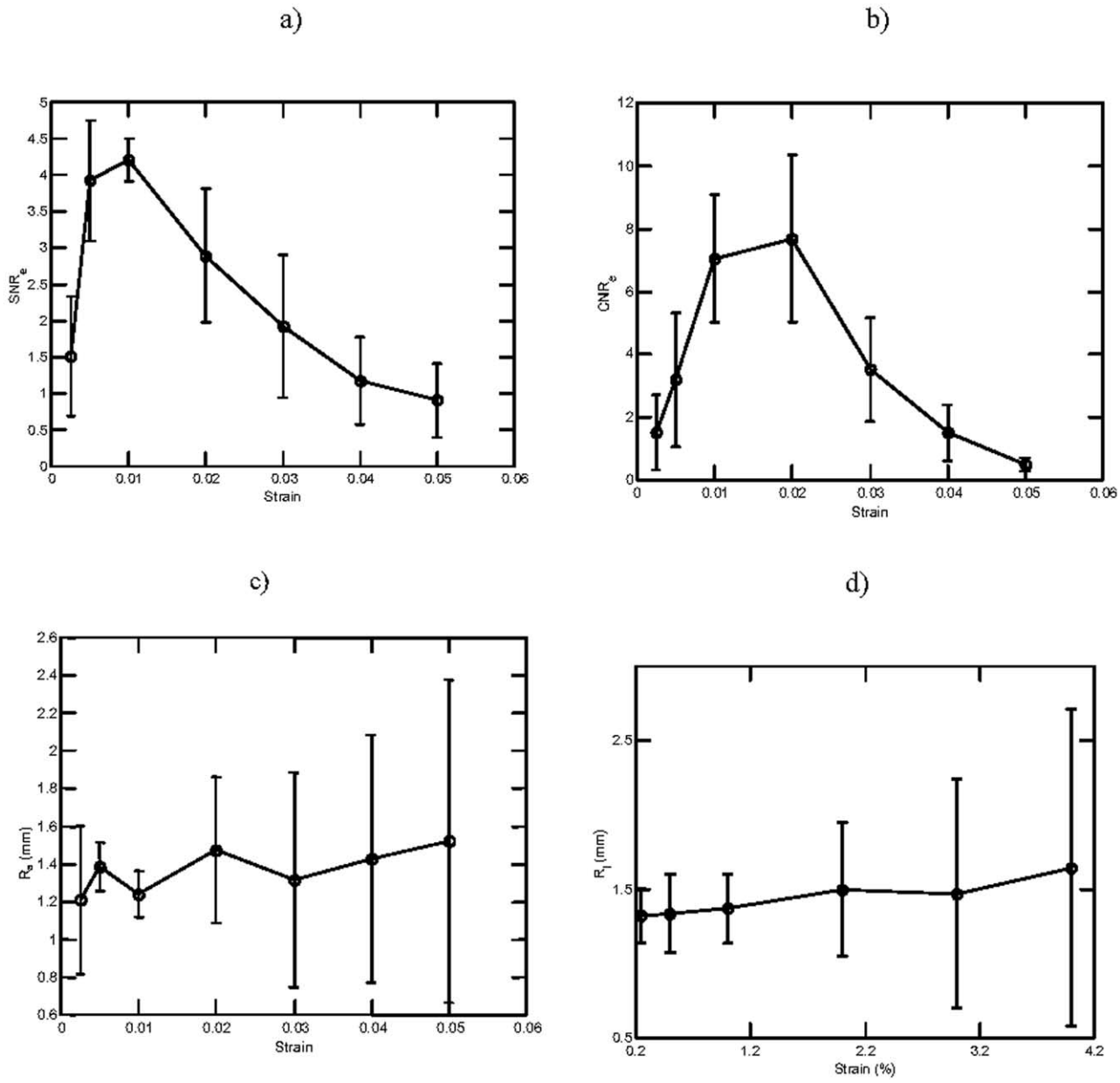

Fig. 5. (a) SNR_e, (b) CNR_e, (c) R_a and (d) R_l as a function of the applied strain ($W = 2$ mm, $\Delta W = 0.2W$). The data points represent the means and the error bars are the SDs over 12 realizations. The expected (theoretical) axial and lateral resolutions are 1.1 mm and 1 mm, respectively.

computed using ANOVA). Such a result is also consistent with eqn (2), as well as with the results obtained by Righetti et al. (2003). Figure 4a shows the SNR_e and Fig. 4b shows the CNR_e plotted as a function of ΔW at a strain of 1% and a W of 2 mm. It can be seen that the SNR_e increases at a less-than-linear rate with respect to ΔW and the CNR_e increases linearly with W ($r > 0.95$). The axial resolution shows a linear dependence on ΔW ($r > 0.95$). These results are consistent with those predicted by the theoretical expressions, eqns (1) and (4). The lateral resolution did not show statistically significant differences for several values of ΔW (p values > 0.05) because the lateral resolution does not depend on the axial strain estimation parameters, as evident from eqn (1).

The applied strain was changed from 0.25% to 5% and the statistics are shown in Fig. 5. The SNR_e and CNR_e show a bandpass-type behavior with respect to the applied strain (Fig. 5a and 5b), which is consistent with prior theoretical and experimental work (Varghese and Ophir 1998; Srinivasan et al. 2003a). The axial as well as the lateral resolu-

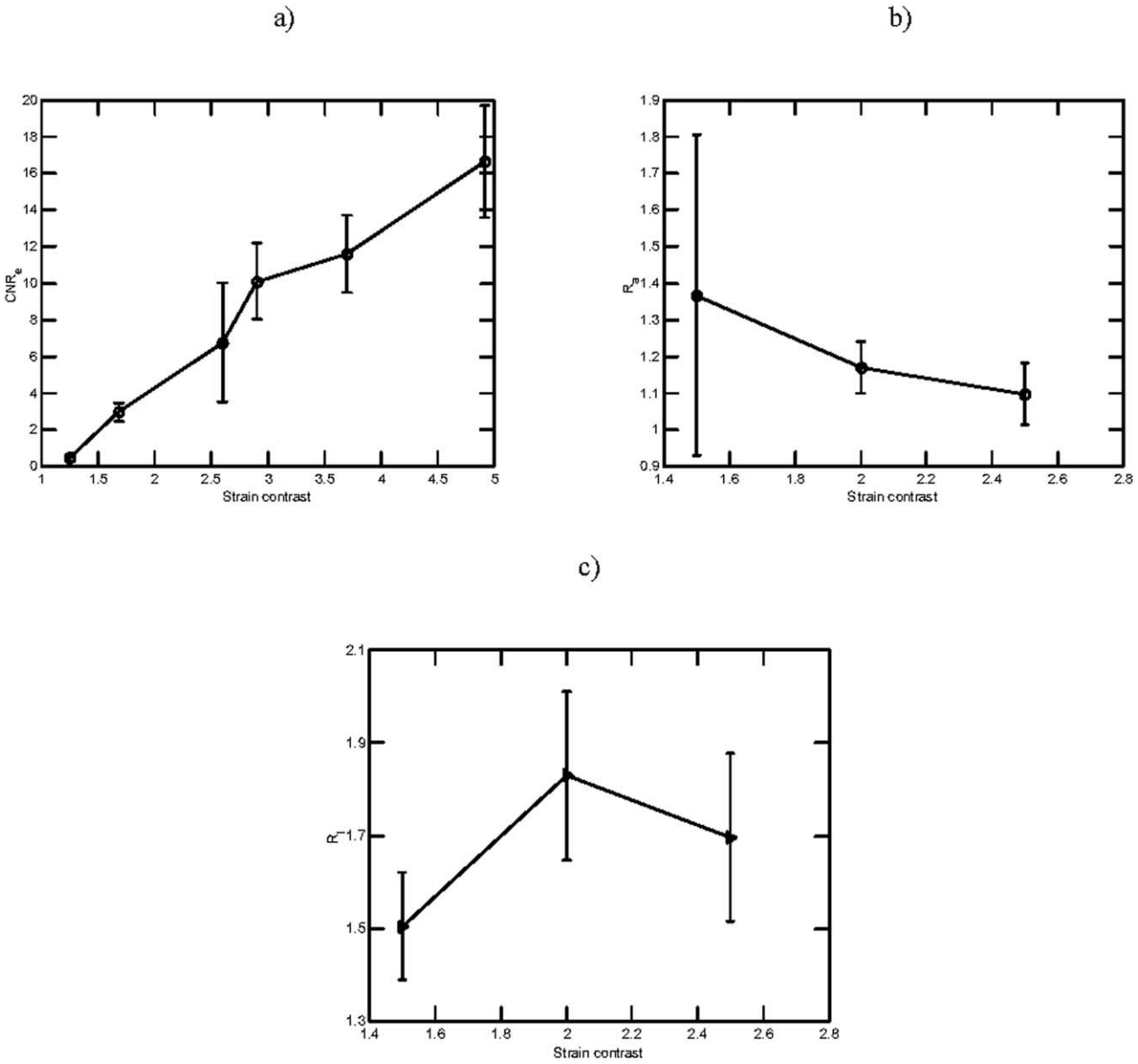

Fig. 6. (a) CNR_e, (b) R_a and (c) R_l as a function of the strain contrast (W = 2 mm, $\Delta W = 0.2W$). The data points represent the means and the error bars are the SDs over four realizations. The actual separation between the inclusions for the lateral resolution study was estimated from the sonograms to be around 1.3 mm.

tions did not show statistically significant changes with the applied strain (p values > 0.05). Note that the uncertainty in the size estimation at large strains is large in comparison with the change in inclusion-separation due to the application of large strains, thereby indicating that changes in the inclusion size due to compression has a minor effect in the accuracy of the estimated inclusion separations. Figure 6 shows the CNR_e, R_a and R_l plotted as a function of the strain contrast. It can be seen that the CNR_e increases with the contrast, as also shown by Varghese and Ophir (1998). The values of R_a and R_l do not show statistically significant differences with contrast, as indicated by eqn (1) and also shown in simulation studies by Righetti et al. (2002) and Righetti et al. (2003).

The results of the resolution study for the schematics shown in Fig. 1b and c are summarized as follows. Figure 7a and b shows sonograms and corresponding elastograms obtained from several consecutive planes acquired across the sample in the elevational direction. Figures 7 and 8 indicate larger inclusion-separations on the elastograms than on the corresponding sonograms. A quantitative comparison

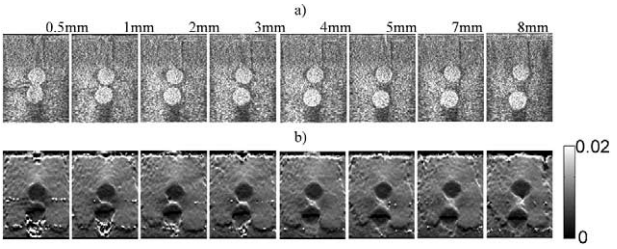

Fig. 7. (a) Sonograms and (b) elastograms of the phantom oriented as shown in the schematic in Fig. 1b, as obtained at several axial separations between the cylindrical cross-sections ($W = 2$ mm, $\Delta W = 0.2W$). For the purpose of illustration, each elastogram is an average over 40 acquisitions.

between the elastographic and sonographic measurements was performed to evaluate the extent of lateral and axial resolution deterioration in the elastographic estimates. Figure 9a and b shows the separations measured from the elastograms plotted as a function of the separations measured from the sonograms.

The elastographic axial as well as lateral measurements did not show significant changes with respect to the sonographic measurements, at different applied strains (p values > 0.05 over 12 realizations), as shown in Fig. 10. Figure 11 shows that the axial and lateral separations on the elastogram with respect to the sonographic measurements at different values of W. The elastographic and sonographic axial resolution estimates were found to be not significantly different from each other (p values > 0.05 over 12 realizations), except for very large values of W, where the axial resolution was significantly deteriorated. Similarly, the elastographic measurements were found to be in good agreement with the sonographic measurements, except for very large W, presumably because of the low elastographic measurement accuracy. Similarly, the axial and lateral separations on the elastogram were not found to be significantly different from the sonographic measurements, for different values of ΔW (p values > 0.05 over 12 realizations) (Fig. 12) as well as for different modulus contrasts (p values > 0.05 over 12 realizations) (Fig. 13).

DISCUSSION

Recent work on the spatial resolution in elastography (Srinivasan et al. 2003a) has shown that the axial resolution is determined by signal processing parameters, such as W and ΔW, provided that the value of W is larger than a threshold that is dictated by the absolute bandwidth of the system. Simulations and theory were used in Srinivasan et al. (2003a) to show the functional dependence of the axial resolution on these signal-processing parameters. The objective of this paper is to validate the prior theoretical and simulation results on the axial resolution as well on the lateral resolution of axial strain elastograms (Righetti et al. 2003). The dependence of the resolution on the mechanical parameters (namely the local strain and the strain contrast) was also studied and it was found that both the axial as well as the lateral resolutions show a weak dependence on the local strain (as well as the strain contrast), as long as the RF signal decorrelation effects due to the local strain were not significant (the signal decorrelation typically occurs at strains larger than 5%). A study of the dependence of the resolution on the sonographic parameters, such as the beamwidth and the bandwidth, was not feasible, due to the unavailability of a multibandwidth and multibeamwidth US system for this work.

Two models, the wedge model and the two-inclusion model, were used for this study. The wedge model facilitated a characterization of the spatial resolution (both axial and lateral) with a single elastogram. However, the geometry of the phantom resulted in stress and strain concentrations, especially in the region between the two inclusions. For example, in Fig. 1, it can be observed that the region enclosed by the two inclusions shows higher strains (brighter) than in those regions that are between the inclusions and the upper and lower boundaries. This artefact improved the strain contrast between the inclusions and the background and, hence, facilitated the detectability of the inclusion edges. The two-inclusion model required obtaining elastograms at several elevational planes because, for every imaging plane, the inclusion cross-sections appear as circular disks. Some strain concentrations due to the lack of plane-strain state conditions (due to the absence of symmetry of the mechanical properties about the imaging plane in the elevational direction) are likely to occur for this model. However, we did not find these strain concentrations to affect the measurements significantly.

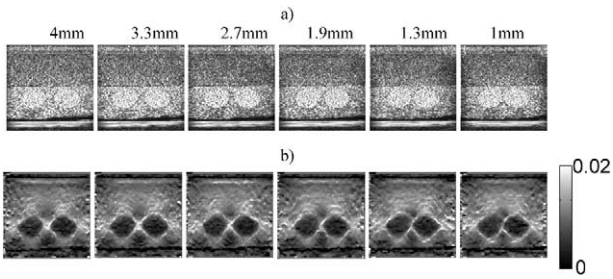

Fig. 8. (a) Sonograms and (b) elastograms of the phantom oriented as shown in the schematic shown in Fig, 1b, at several lateral separations between the cylindrical cross-sections ($W = 2$ mm, $\Delta W = 0.2W$). For the purpose of illustration, each elastogram is an average over 40 acquisitions.

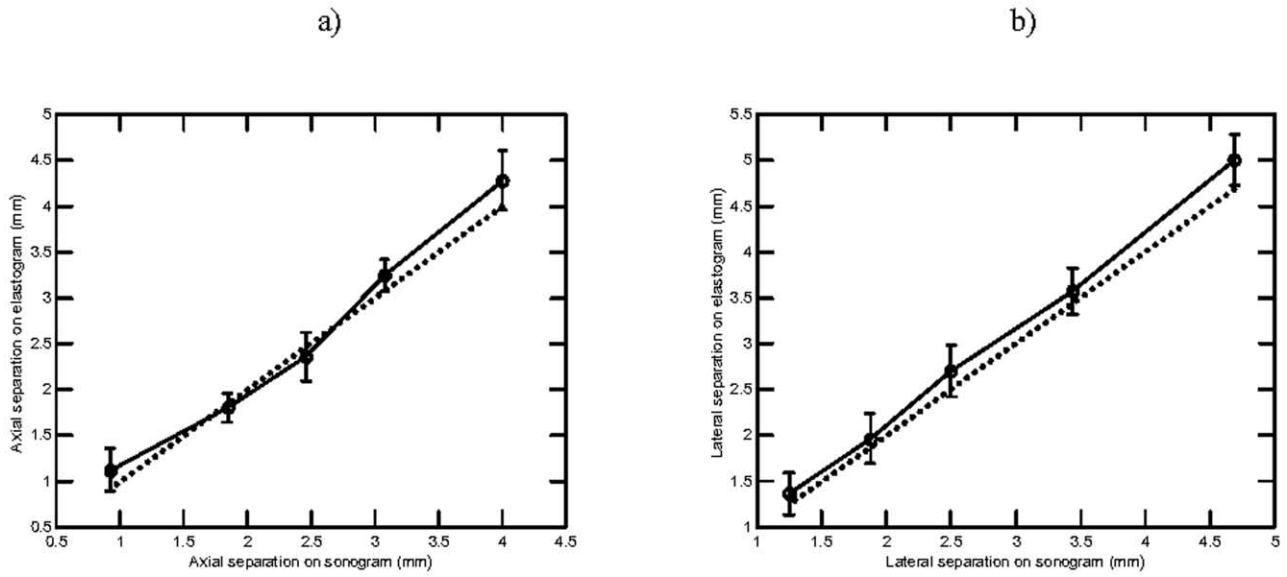

Fig. 9. Elastographic (a) axial separation and (b) lateral separation measurements, plotted as a function of the separations evaluated from the corresponding sonograms ($W = 1$ mm, $\Delta W = 0.2W$). Twelve realizations were used to compute the statistics. The dotted lines represent the 45° line (i.e., the sonographic separation plotted as a function of itself).

The experimental results were in good agreement with the theoretical and simulation results reported in Srinivasan et al. (2003a) for values of W greater than 1 mm. The experimental results were not computed for separations smaller than 0.5 mm, due to difficulties in controlling separations smaller than around 0.5 mm in all realizations. Moreover, due to measurement noise in the experiments, the results for separations of 0.5 mm were not found to be reliable. The variations in the inclusion separations at each imaging plane in the 12 experimental realizations were around 0.25 mm. Hence, we only considered separations of more than 1 mm. The elastograms were found to show larger separations than the corresponding sonograms. This is because the elastographic resolution can be expected to be the poorest of the mechanical and the sonographic resolutions (because the

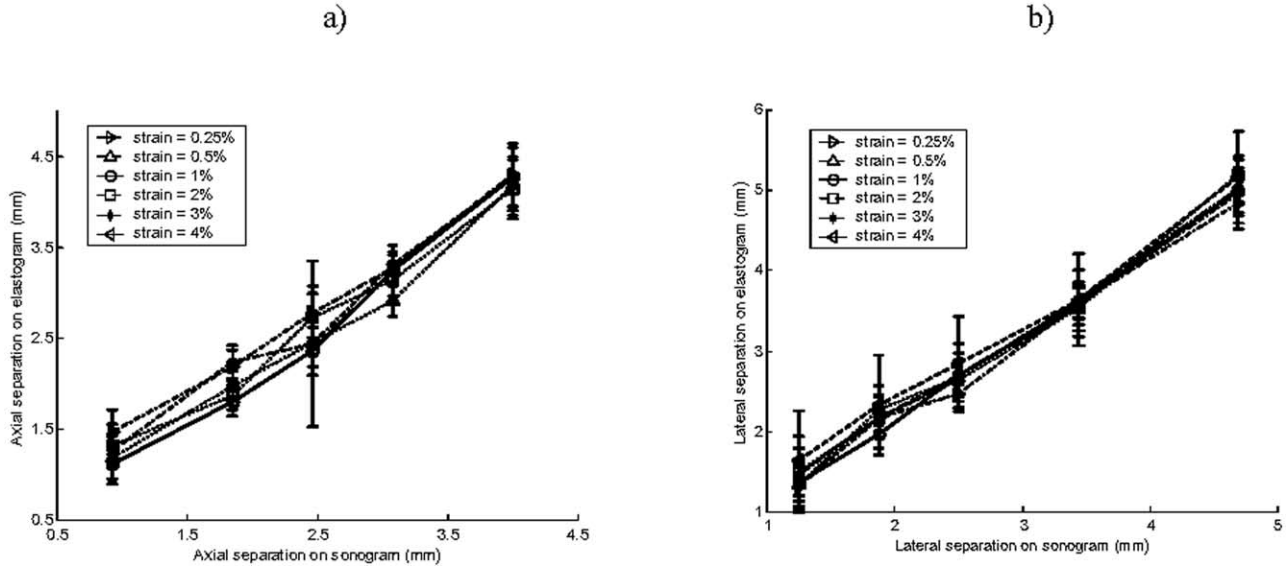

Fig. 10. Elastographic (a) axial separation and (b) lateral separations plotted as a function of the corresponding sonographic measurements, obtained at several applied strains ($W = 1$ mm, $\Delta W = 0.2W$).

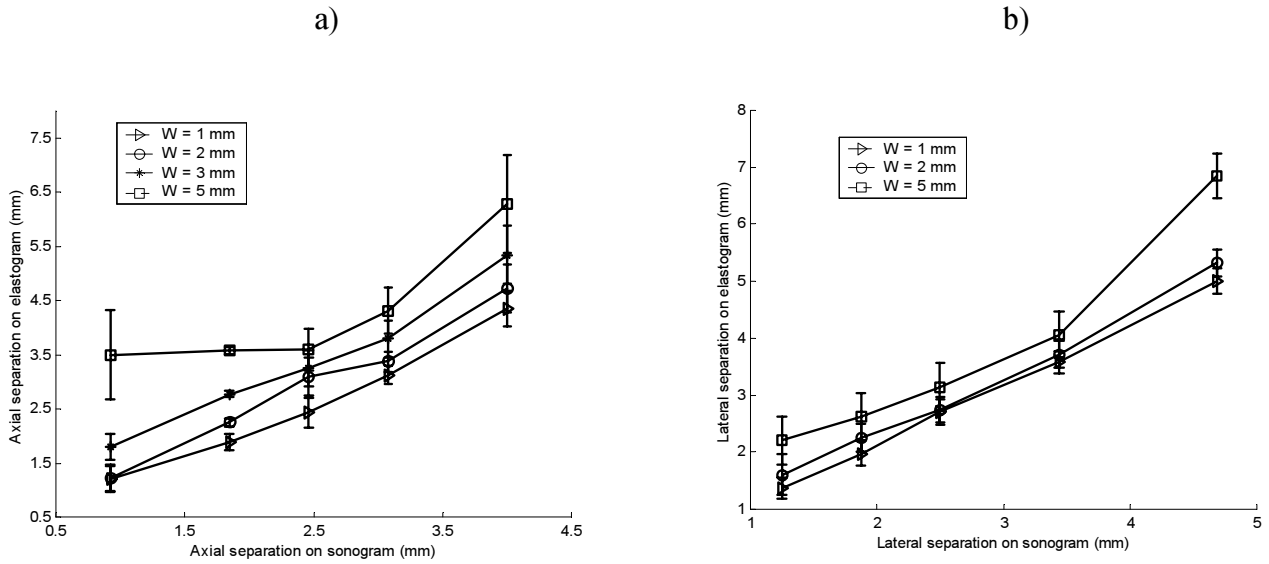

Fig. 11. Elastographic (a) axial separation and (b) lateral separations plotted as a function of the corresponding sonographic measurements, obtained by processing the elastograms with several window lengths ($\Delta W = 0.2W$, applied strain = 1%).

elastogram is a result of mechanical motion measured using sonography).

The phantom models used in this work utilized sponges in gelatin-agar mixtures. The use of open cell sponges with different elastic moduli in elastrographic phantom applications was reported by Ophir et al. (1991). The use of gelatin mixtures at different concentrations for the inclusions and the background are prevalent in the literature (Kallel et al. 2001; Hall et al. 1997). Such phantoms exhibit a time-dependence of the modulus contrast and size, due to diffusion caused by concentration gradients between the materials that constitute the background and the inclusion. Moreover, the time taken to stabilize such phantoms is measured in months. In this study, we used sponge reinforced phantoms to provide stable values of con-

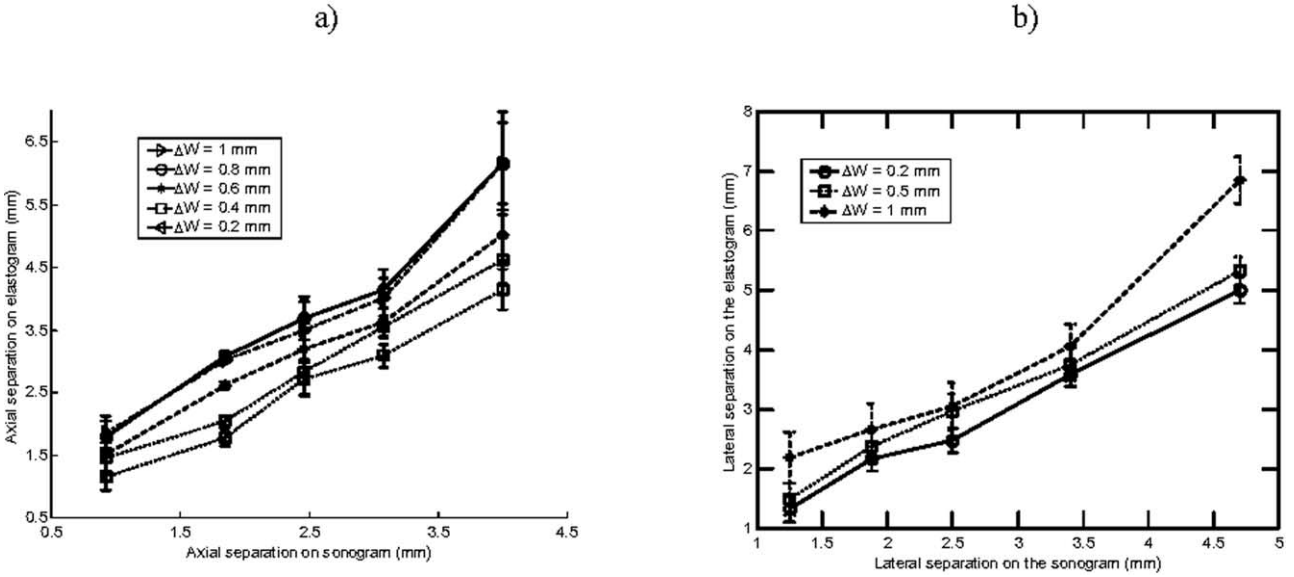

Fig. 12. Elastographic (a) axial separation and (b) lateral separations plotted as a function of the corresponding sonographic measurements, obtained by processing the elastograms with several ΔW values (W = 1 mm, applied strain = 1%).

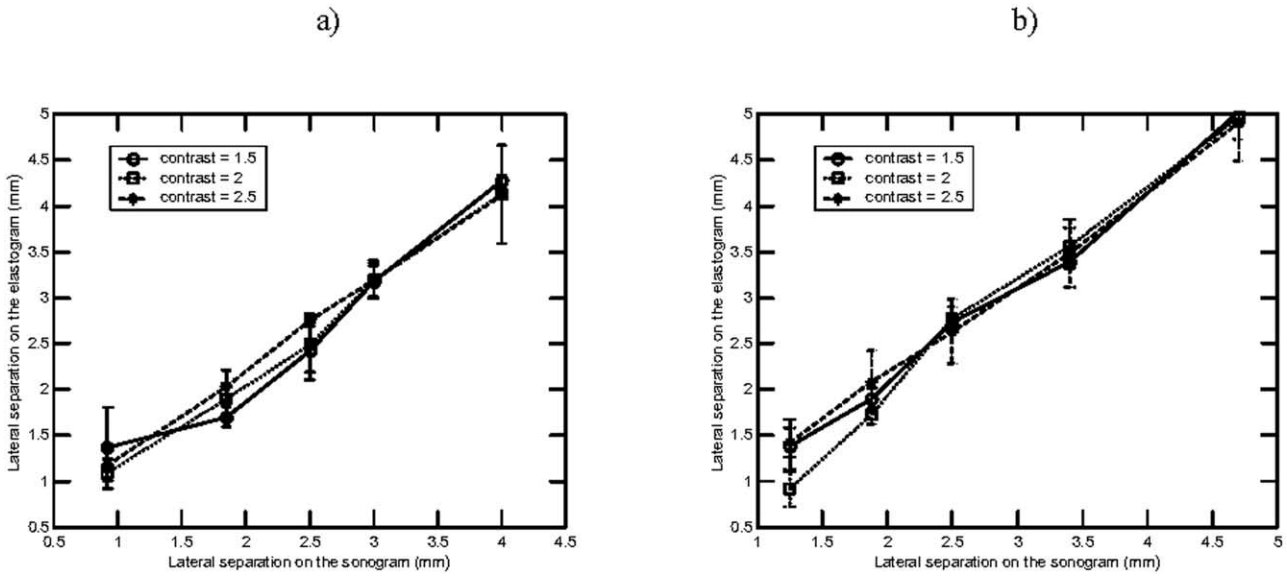

Fig. 13. Elastographic (a) axial separation and (b) lateral separations plotted as a function of the corresponding sonographic measurements, obtained for different lesion-background strain contrasts ($W = 1$ mm, $\Delta W = 0.2W$, applied strain = 1%).

trast and spatial resolution over several days. Air was carefully removed from the sponge samples by squeezing them in hot water before and after mixing the gelatin-agar mixture. These sponge reinforced phantoms offer the advantages of obtaining high modulus contrasts and sharp boundaries and ease of making very small cross-sections. The disadvantages of such phantoms are difficulty in removing air bubbles, the nonhomogeneity within the sponge material and the dependence of the modulus on the amount of the sponge material. We expect micrometer-sized bubbles to be present in the sponge reinforced gelatin phantoms if the sponges are not degassed adequately.

CONCLUSION

An experimental characterization of the axial and lateral resolution of axial strain elastograms was conducted. The experimental axial and the lateral resolutions of the strain elastograms were found to be greater than 1 mm for a 5-MHz, 60% fractional bandwidth, 1-mm beamwidth transducer. The axial resolution was found to deteriorate linearly with respect to the window length and the window shift used for strain estimation, as predicted by previous theoretical studies. The lateral resolution was found to be relatively insensitive to these algorithmic parameters. Both the axial as well as the lateral resolutions were found to be relatively insensitive to mechanical parameters, such as the applied strain or the lesion-background modulus contrast, for the parameter ranges that were considered in this study. A close correspondence between the separation of the inclusions in the sonograms and the elastograms was found. The elastograms overestimated the sonographic separations by approximately 5%.

Acknowledgements—This work was supported by the National Cancer Institute program (project P01-CA64597) awarded to the University of Texas Medical School, Houston.

REFERENCES

Alam SK, Ophir J, Varghese T. Axial resolution criteria in elastography: An empirical study. IEEE Trans Ultrason Ferroelec Freq Control 2000;47(1):304–309.

Bendat JS, Piersol AG. Random data: Analysis and measurement. 2nd ed. New York: John Wiley and Sons, 1986.

Bilgen M, Insana MF. Predicting target detectability in acoustic elastography. IEEE Ultrason Symp 1997;2:1427–1430.

Céspedes I. Elastography: Imaging of biological tissue elasticity. Ph.D. dissertation. University of Houston, 1993.

Cook LT, Zhu Y, Hall TJ, Insana MF. Bioelasticity imaging II. Spatial resolution. Proc SPIE Med Imaging 2000;3982:315–324.

Hall TJ, Insana MF, Krouskop T. Phantom materials for elastography. IEEE Trans Ultrason Ferroelec Freq Control 1997;44: 1355–1365.

Kallel F, Prihoda CD, Ophir J. Contrast-transfer efficiency for continuously varying tissue moduli: Simulation and phantom validation. Ultrasound Med Biol 2001;27(8):1115–1125.

Liu J, Insana MF. Spatial resolution in elasticity imaging: IEEE International Ultrasonics Symposium, October 5–8, Hawaii, 2003.

Ophir J, Alam SK, Garra B, et al. Elastography: Ultrasonic estimation and imaging of the elastic properties of tissues. Proc Inst Mech Eng Part H 1999;213:203–233.

Ophir J, Céspedes I, Ponnekanti H, Yazdi Y, Li X. Elastography: A quantitative method for imaging the elasticity of biological tissues. Ultrason Imaging 1991;13:111–134.

Righetti R, Ophir J, Ktonas P. Axial resolution in elastography. Ultrasound Med Biol 2002;28(1):101–113.

Righetti R, Srinivasan S, Ophir J. Lateral resolution in elastography. Ultrasound Med Biol 2003;29(5):695–704.

Srinivasan S, Ophir J. A zero-crossing strain estimator for elastography. Ultrasound Med. Biol 2003;29(2):227–238.

Srinivasan S, Kallel F, Ophir J. The effects of digitization on the elastographic signal-to-noise ratio. Ultrasound Med Biol 2002a; 28(11):1521–1534.

Srinivasan S, Kallel F, Souchon R, Ophir J. Analysis of an adaptive strain estimation technique in elastography. Ultrason Imaging 2002b;24:109–118.

Srinivasan S, Krouskop T, Ophir J. Comparing elastographic strain images with modulus images obtained using nanoindentation: Preliminary results using phantoms and tissue samples. Ultrasound Med. Biol 2004;03(3):329–343.

Srinivasan S, Righetti R, Ophir J. Trade-offs between axial resolution and signal-to-noise ratio in elastography. Ultrasound Med Biol 2003;29(6):847–866.

Varghese T, Ophir J. A theoretical framework for performance characterization of elastography: The strain filter. IEEE Trans Ultrason Ferroelec Freq Control 1997;44(1):164–172.

Varghese T, Ophir J. An analysis of elastographic contrast-to-noise ratio. Ultrasound Med Biol 1998;24(6):915–924.